

Study of bound states in ^{12}Be through low-energy $^{11}\text{Be}(\text{d},\text{p})$ -transfer reactions

J. G. Johansen,^{1,2} V. Bildstein,³ M. J. G. Borge,^{4,5} M. Cubero,⁵ J. Diriken,^{6,7} J. Elsevier,⁶ L. M. Fraile,⁸ H. O. U. Fynbo,¹ L. P. Gaffney,⁹ R. Gernhäuser,¹⁰ B. Jonson,¹¹ G. T. Koldste,¹ J. Konki,^{4,12,*} T. Kröll,² R. Krücken,^{10,13} D. Mücher,¹⁰ T. Nilsson,¹¹ K. Nowak,¹⁰ J. Pakarinen,^{4,12,*} V. Pesudo,⁵ R. Raabe,⁶ K. Riisager,¹ M. Seidlitz,¹⁴ O. Tengblad,⁵ H. Törnqvist,^{4,11} D. Voulot,⁴ N. Warr,¹⁴ F. Wenander,⁴ K. Wimmer,^{10,15} and H. De Witte⁶

¹*Department of Physics and Astronomy, Aarhus University, DK-8000 Aarhus C, Denmark*

²*Institut für Kernphysik, Technische Universität Darmstadt, D-64289 Darmstadt, Germany*

³*Department of Physics, University of Guelph, Guelph, Ontario, Canada N1G2W1*

⁴*CERN, CH-1211 Genève, Switzerland*

⁵*Instituto de Estructura de la Materia, CSIC, E-28006 Madrid, Spain*

⁶*Instituut voor Kern- en Stralingsfysica, KU Leuven, 3001 Leuven, Belgium*

⁷*Belgian Nuclear Research Centre SCK-CEN, Boeretang 200, B-2400 Mol, Belgium*

⁸*Grupo de Física Nuclear, Universidad Complutense, CEI Moncloa, E-28040 Madrid, Spain*

⁹*Oliver Lodge Laboratory, University of Liverpool, L69 7ZE, England, UK*

¹⁰*Physik Department E12, Technische Universität München, 85748 Garching, Germany*

¹¹*Fundamental Fysik, Chalmers Tekniska Högskola, S-41296 Göteborg, Sweden*

¹²*Helsinki Institute of Physics, PO box 64, FI-00014 Helsinki, Finland*

¹³*TRIUMF, Vancouver BC, V6T 2A3, Canada*

¹⁴*Institut für Kernphysik, Universität zu Köln, D-50937 Köln, Germany*

¹⁵*Department of Physics, Central Michigan University, Mount Pleasant, Michigan 48859, USA*

(Dated: June 6, 2019)

The bound states of ^{12}Be have been studied through a $^{11}\text{Be}(\text{d},\text{p})^{12}\text{Be}$ transfer reaction experiment in inverse kinematics. A 2.8 MeV/u beam of ^{11}Be was produced using the REX-ISOLDE facility at CERN. The outgoing protons were detected with the T-REX silicon detector array. The MINIBALL germanium array was used to detect gamma rays from the excited states in ^{12}Be . The gamma-ray detection enabled a clear identification of the four known bound states in ^{12}Be , and each of the states has been studied individually. Differential cross sections over a large angular range have been extracted. Spectroscopic factors for each of the states have been determined from DWBA calculations and have been compared to previous experimental and theoretical results.

PACS numbers: 25.60.Je, 21.10.Jx, 21.10.Tg, 27.20.+n, 23.20.-g

I. INTRODUCTION

The structure of the light neutron-rich nuclei has presented many challenges during the last decades [1] and this area of the nuclear chart is a prime region for investigations of halos [2–4], cluster states [5], unbound systems [6, 7] as well as the vanishing of shells [8]. A key question in these topics is the spectroscopic composition of the bound states, which can be accessed experimentally in complementary ways [9–11]. We are here concerned with the structure of the bound states in ^{12}Be . The states are probed via transfer reactions. This method has recently been employed also for the study of other exotic nuclei [12–14]. In neither of the neighboring isotopes ^{11}Li and ^{11}Be can the ground states be written as a simple single-particle configuration (see [15] and the references above). This seems to also be the case for ^{12}Be .

Four bound states are presently known in ^{12}Be , see Fig. 1. The highest lying bound state (1_1^-) has an excitation energy of only $E^* = 2.70$ MeV. Hence the level density in ^{12}Be is relatively high. This high level den-

sity is believed to be due to configurations from both the $0p_{1/2}$ -shell and the $1s_{1/2}0d_{5/2}$ -shell, a mixing which is also known to occur in ^{11}Be . This mixing was first suggested in 1976 by Barker [16] following a β -decay study of ^{12}Be . Further experimental support for this suggestion has come through measurements of transition strengths to the 1_1^- [17], 0_2^+ [18, 19] and 2_1^+ bound states [20], through extraction of the ground state charge radius [21] and through nuclear knock out [22], break-up [23, 24], transfer [25] and charge exchange [26] reactions. These measurements have shown that the $N=8$ magic number is clearly broken in ^{12}Be and the detailed mixing of the shells is still being investigated. The short lifetime combined with the narrow separation of the bound states has made it difficult to study these states individually.

^{11}Be is a well known 1-neutron halo nucleus. This large separation of the ^{10}Be and the halo-neutron in ^{11}Be has led to an interpretation of ^{12}Be as having a three-particle structure with a ^{10}Be core and two neutrons, e.g. [27]. The 1_1^- state is particularly interesting in a three-body model. This state is only 1 MeV below the two-neutron threshold and is expected to be a two-neutron halo in the three-body model with one neutron in an s state and the other in a $p_{1/2}$ state. A fifth bound state that differs from the 1_1^- state only in spin coupling has

* Present address: University of Jyväskylä, Jyväskylä FI-40014, Finland

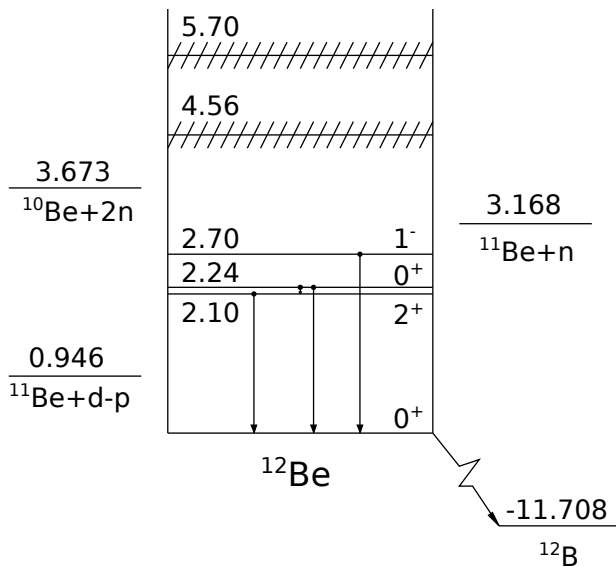


FIG. 1. The level scheme of ^{12}Be containing the known states and resonances as well as the gamma decay transitions for the bound states. The values for the bound states and the resonances are taken from [17–19, 33].

been suggested: a 0_1^- state with an excitation energy around $E^* = 2.5$ MeV [28]. However, this state has never been seen experimentally.

Several other models have been used to predict the ^{12}Be structure: apart from shell models and a simple wavefunction ansatz [29], antisymmetrized molecular dynamics [30], the deformed potential model [31], as well as the generator coordinate method and no core shell model [32] have all been employed.

The first studies of excited states in ^{12}Be were in transfer reactions, mainly $^{10}\text{Be}(t,p)^{12}\text{Be}$, these results are summarized in Fortune et al. [33]. Most recent studies have been in break-up reactions, and also a $^{11}\text{Be}(d,p)^{12}\text{Be}$ transfer reaction has been performed at TRIUMF by R. Kanungo et al. [25]. Spectroscopic factors were determined in the latter for all four bound states. The value for the 0_2^+ state was only given with a large uncertainty, due to the inability to clearly distinguish it from the 2_1^+ state. The spectroscopic factors determined in the experiment at TRIUMF have later been questioned, since it disagreed with theoretic calculations [29].

In this paper, we report on a $^{11}\text{Be}(d,p)$ -experiment performed at ISOLDE. The set-up represents an improvement upon an earlier $^9\text{Li}(d,p)$ experiment [34] as both gamma rays and charged particles were measured, enabling a clear identification of all the bound states in ^{12}Be . Hence, detailed studies of each state have been made and spectroscopic factors have been determined for all the four states. The lifetime and the branching ratio of the decay of the 0_2^+ state have also been determined. Results from the other reaction channels as well as on the unbound resonances in ^{12}Be [35] will be reported else-

where.

The paper starts with a description of the experimental setup and experimental procedure, section II. The analysis of the data is described in section III. The focus of the analysis is the identification of the individual states, but the lifetime of and the branching ratio for the decay of the 0_2^+ state is also given. The analysis is done in three steps described in section III. The determined differential cross sections are presented along with the DWBA calculations in section IV. The spectroscopic factors are also presented and discussed in this section. The paper ends with a short summary and conclusion in section V.

II. THE EXPERIMENTAL PROCEDURE

The experiment was performed at the ISOLDE facility, CERN, Switzerland. The ^{11}Be activity was produced by a 1.4 GeV proton beam through fragmentation of a uranium carbide target. The Be atoms were subsequently ionized via laser ionization [36], mass separated and led to the REX-ISOLDE post-accelerator. Here they were bunched in REXTRAP, fully stripped to charge state +4 in REXEBIS and finally post-accelerated to 2.8 MeV/u (30.7 MeV) in the REX linear accelerator [37]. The beam intensity after post-acceleration fluctuated between $4.4 \times 10^6/\text{s}$ and $1 \times 10^7/\text{s}$. This led to a total number of ^{11}Be nuclei of $N_{^{11}\text{Be}} = 1.11(25) \times 10^{12}$. The beam intensity was determined by Coulomb scattering on a silver target, which was performed regularly during the experiment. The fluctuation in the beam intensity was monitored via the rate of detected particles (p, d and t) throughout the experiment. The set-up allowed for a study of several properties of the secondary ^{11}Be beam. The beam spot was determined to be approximately 5 mm in diameter, details in [38].

A deuterated polyethylene (CD_2) target was used in the experiment. The thickness of the target was 1.00(5) mg/cm². Runs on a pure carbon target and a regular polyethylene target (CH_2) were performed and provided information about reactions on C and H in the primary target.

A setup specialized for transfer reaction experiments at ISOLDE was used. The setup consisted of the MINIBALL germanium detector array [40, 41] in combination with the T-REX silicon detector setup [42]. The T-REX was used to detect the light charged particles from the reaction. The T-REX consisted of 12 silicon telescope detectors placed to cover angles from 8° to 152° in the laboratory and with an almost 2π -azimuthal angular coverage. A drawing of the T-REX is seen in Fig. 2A. Fig. 2B shows the angles and energies covered by the T-REX (grey area). The dashed lines represents the energy required for a proton to pass through the first of the telescope detectors. The kinetic curves of the four known bound states are also shown in Fig. 2B. Particle identification through $\Delta E - E$ plots can be performed above the dashed lines. Particles with energy less than

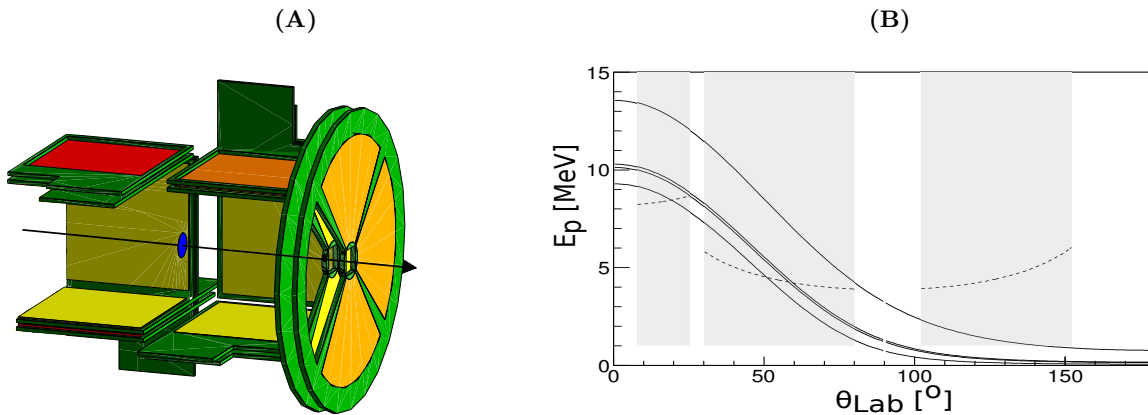


FIG. 2. A: A drawing of the T-REX silicon array [42]. The three detectors on the left side are omitted to clear the view inside the T-REX. B: The kinetic curves for the emitted protons in a $^{11}\text{Be}(d,p)^{12}\text{Be}$ reaction (solid lines). Each line corresponds to a population of one of the four bound states, Fig. 1. The gray area represents the angles and energies covered by the T-REX and the dashed line corresponds to the minimum energy required for $\Delta E - E$ -identification.

1 MeV could not be separated from the noise level.

The gamma-ray detection provided by the MINIBALL was required to separate the bound states in ^{12}Be . The MINIBALL consists of 24 germanium detectors placed in eight clusters. The clusters were placed to cover a wide angular range. The germanium detectors had an energy range up to 8 MeV. The energy-dependent detection efficiency was determined using three gamma sources (^{152}Eu , ^{60}Co and ^{207}Bi) and gamma rays from β -decay of ^{11}Be . The ^{11}Be beam used for the efficiency calculation was stopped in an aluminum foil at the target position. The detection efficiencies for decays occurring at the target position are given, for the relevant decays, in Table I. More details on the experimental procedures can be found in [39].

III. IDENTIFICATION OF THE BOUND STATES IN ^{12}Be

The identification of the four bound states in ^{12}Be is performed in three steps. The protons are identified in a $\Delta E - E$ plot if the energy of the particles is sufficiently high (section III A). This is only the case for the forward laboratory angles according to Fig. 2B. The excited states are identified using gating on gamma-ray energies (gamma gates) afterwards. The identification of (d,p)-

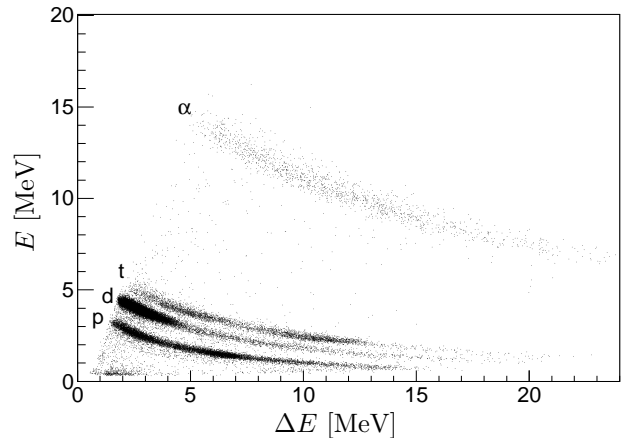


FIG. 3. A $\Delta E - E$ -plot for a strip in one of the detectors covering the forward laboratory angles. The three curves corresponding to p, d and t are clearly separated.

Decay	E_γ [keV]	ϵ [%]
$0_2^+ \rightarrow 2_1^+$	144	16.2(5)
$0_2^+ \rightarrow 0_1^+$	511 (pair creation)	8.2(5)
$2_1^+ \rightarrow 0_1^+$	2107	3.5(2)
$1_1^- \rightarrow 0_1^+$	2680	3.0(2)

TABLE I. The γ -energy and the MINIBALL detection efficiency for the four main γ -decay lines in ^{12}Be .

reactions from particles stopped in the ΔE -detectors is divided in two, forward and backward angles. In forward angles only protons populating ^{12}Be in an excited state will be stopped in the ΔE -detector, Fig. 2B. These protons can be identified using gamma gates (section III C). Protons populating the ground state will have sufficient energy to penetrate the ΔE -detector in the forward angle and can be ignored when analyzing particles stopped in the forward ΔE -detectors. In backward laboratory angles only protons populating the ground state and particles from reactions on carbon in the target have sufficient energy to be separated from the noise level. The latter can be taken into account via the runs on a pure carbon target (section III D).

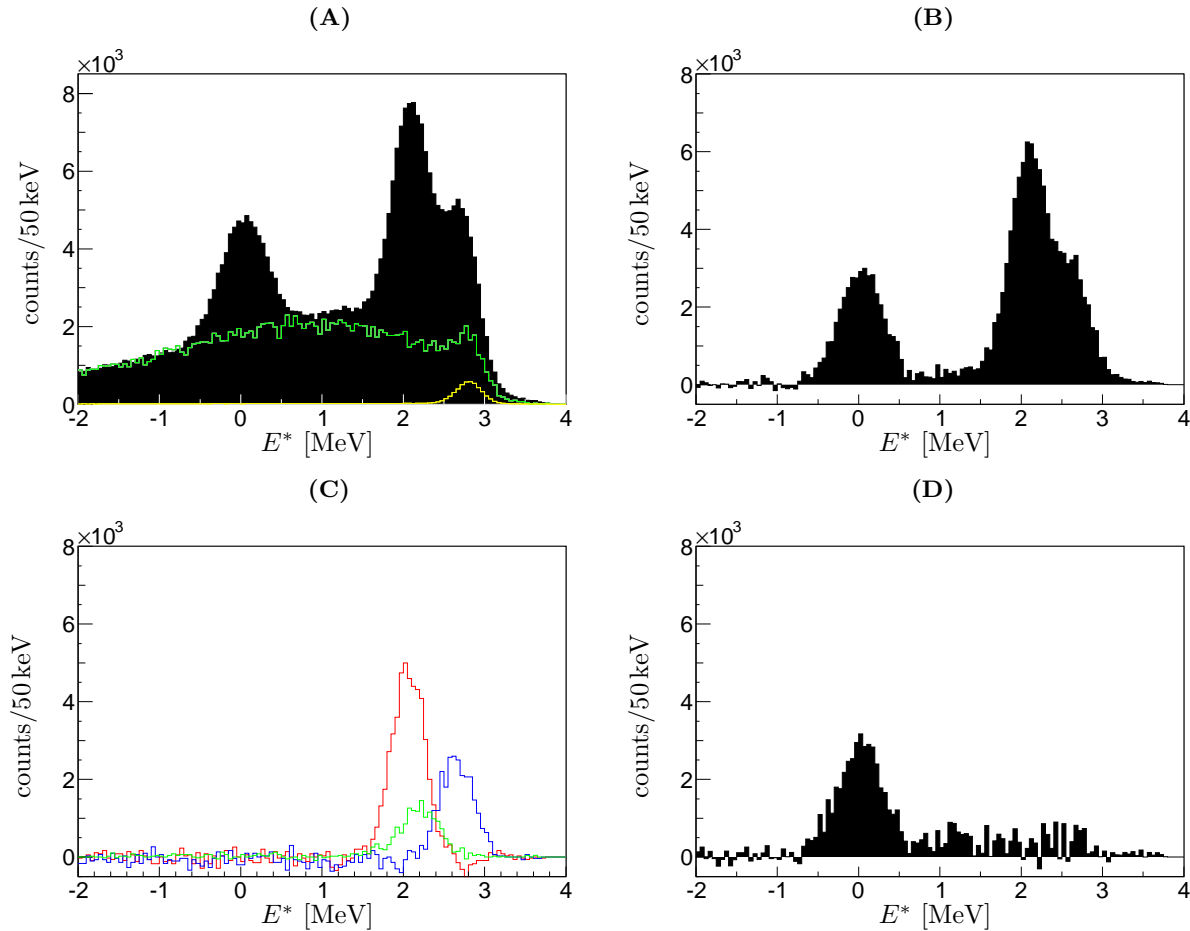


FIG. 4. Four plots showing the excitation energy of ^{12}Be . A: The excitation energy spectrum determined from the momentum of protons identified from the $\Delta E - E$ -plots (Black) along with the background spectra determined from runs on the carbon target (green) and the CH_2 target (yellow). B: The excitation energy spectrum from (A) with the two background spectra subtracted. C: Excitation energy spectra determined from protons gated on the gamma-lines shown in Fig. 5; red: 2_1^+ , green: 0_2^+ and blue: 1_1^- . D: The excitation energy spectrum from (B) with the three gamma gated spectra in (C) subtracted only the ground state peak is present.

A. Particles stopped in the E -detector

Fig. 3 shows a $\Delta E - E$ plot for one strip in one of the detectors covering the forward laboratory angles. Protons, deuterons, tritons and α -particles are easily identified. A gate is made to select the protons. Similar plots and gates have been made for each strip separately.

The excitation energy spectrum for ^{12}Be is obtained using the kinematics of the identified protons, Fig. 4A. A large part of the protons stems from reactions on C and H in the target. The background is determined by analyzing the data from the runs on the pure carbon and the regular polyethylene target, and is indicated by the green and yellow line in Fig. 4A. Fig. 4B shows the ^{12}Be excitation energy spectrum with the backgrounds subtracted. The ground state of ^{12}Be is clearly identified as the peak at 0 MeV. There is still a small additional background component at 1 MeV, which might extend into the ground state peak. Only the background from C and

H in the target are taken into account when determining the ground state differential cross section, and the additional background will lead to an extra uncertainty in the final spectroscopic factors, section IV. The 2_1^+ - and the 1_1^- states are also visible in the spectra, but the energy resolution is too poor to separate the two or to see the 0_2^+ state at 2.24 MeV and gamma gates are required to identify these states. Gammagates have been determined from the spectra in Fig. 5, which is described below. The gamma gates have been applied and the spectra for the three excited states are shown in Fig. 4C. Fig. 4D shows the total excitation energy spectrum with efficiency corrected background and gamma gated spectra subtracted. This spectrum should thus represent the ground state of ^{12}Be . Only few events with $E^* > 0.6$ MeV are observed in Fig. 4D. This shows that almost every event in the total spectrum can be described either from reactions on C and H in the target or from (d,p)-reactions.

The gamma gates for Fig. 4C are determined from

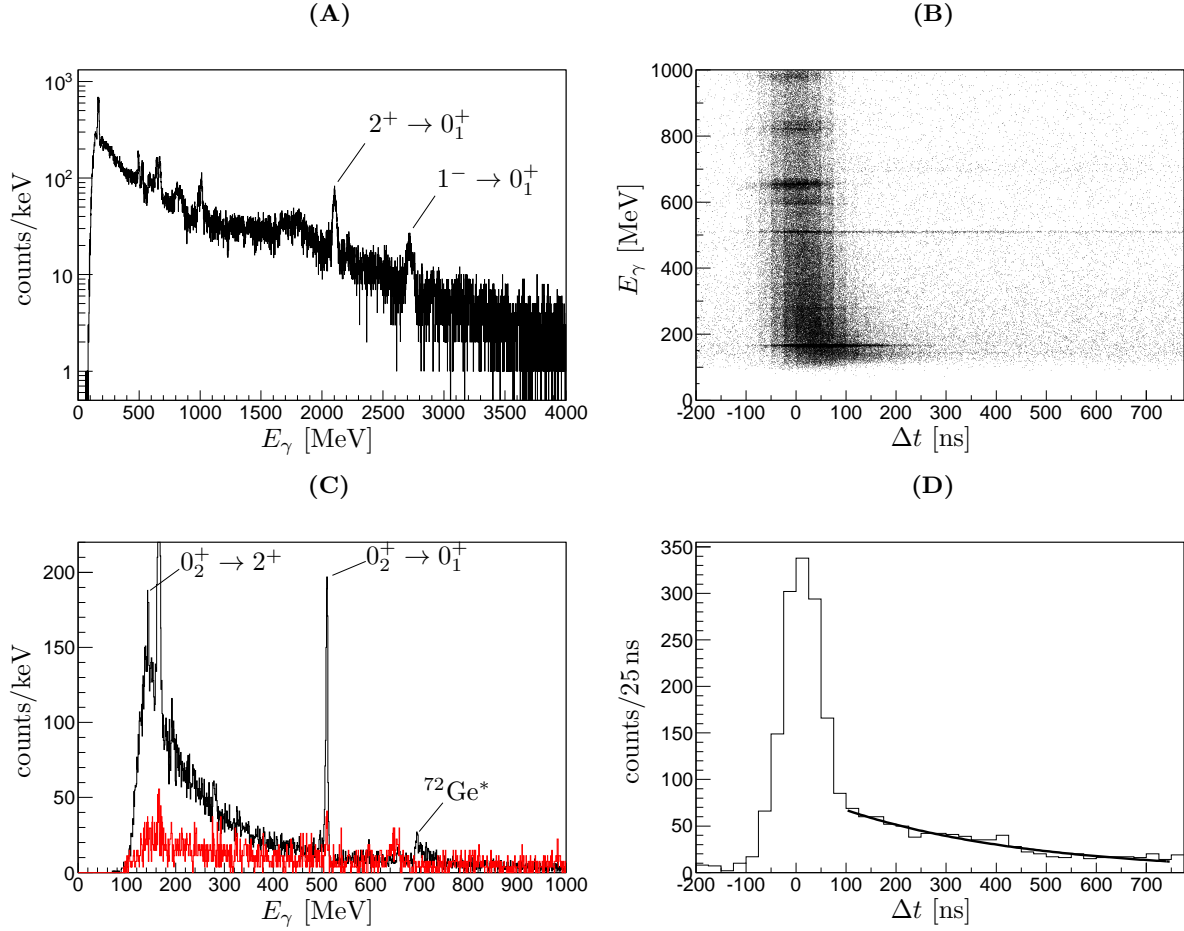


FIG. 5. Spectra for gammas in coincidence with identified protons. A: Doppler-corrected energy spectrum. B: The laboratory gamma energy vs. the time difference between the detected proton and the detected gamma ($\Delta t = t_\gamma - t_p$). C: The laboratory gamma energy spectrum before the reaction ($\Delta t < -75$ ns) (red) and after the reaction ($\Delta t > 100$ ns) (black). D: The time difference between the detected gamma and the detected proton for gammas in the peak at 509.6 keV along with the fit to an exponential decay used to determine the lifetime of the 0_2^+ state.

two spectra, Fig. 5A+C. A gamma-ray energy spectrum is produced using gamma rays in coincidence with the identified protons, Fig. 5A. The energy is corrected for Doppler-shift, due to the emission from a moving nucleus. Peaks at 2103 keV and at 2722 keV are clearly seen. The two peaks are from the decay of the 2^+ - and the 1^- state to the ground state respectively, see Fig. 1 and Table I. Gates are set on the two peaks and excitation energy spectra of ^{12}Be are generated using protons in coincidence with gammas within these gates, Fig. 4C (red and blue). The two spectra are scaled with $1/\epsilon$ from Table I to take the MINIBALL detection efficiency into account. The two peaks are situated at 2061 ± 202 keV and 2658 ± 192 keV respectively validating the interpretation that the gamma gated protons stem from the population of the 2_1^+ and the 1_1^- states.

The 0_2^+ state is long lived, the lifetime of the state was determined to be $\tau = 331(17)$ ns by Shimoura et al. [19]. The excited ^{12}Be nuclei are either stopped within the setup or far away from the MINIBALL detectors be-

fore decaying. Only gammas from ^{12}Be nuclei stopped within the setup can be detected for the 0_2^+ state. The nuclei are stopped in the forward silicon detectors or in the frame holding the detectors. This requires an outgoing angle larger than 7° for the ^{12}Be nucleus, which corresponds to center of mass angles between 71° and 122° for the protons. Within this area the gamma gate should hold, but fluctuations in the beam would lead to a larger uncertainty close to the limits, as some ^{12}Be nuclei might not be stopped. The events populating the long lived 0_2^+ state can be identified by looking at time delayed gammas. Fig. 5B shows the time between the detected gamma and the detected proton (Δt) against the laboratory gamma energy. The laboratory gamma energy is used, as the gammas of interest come from stopped nuclei. Events with $|\Delta t| < 75$ ns is considered prompt decays and events with $|\Delta t| > 100$ ns is considered delayed gamma decays. The spectra in Fig. 5C shows a projection onto the gamma energy axis before (red) and after (black) the reaction. A peak at 166 keV is present

both before and after the reaction and stems from an unknown background. The reaction leads to an increase in the overall background, but three new peaks emerge after the reaction. Two narrow and one broad. The mean value and width of the three peaks are determined using a Gaussian fit: 143.5 ± 2.7 keV, 509.6 ± 2.5 keV and 709 ± 23 keV. The first two are identified as the decays of the 0_2^+ state, see Table I. The last one stems from decay of excited ^{72}Ge within the MINIBALL detector. The germanium isotopes are excited through inelastic scattering with neutrons and decay subsequently [43, 44].

The two time delayed peaks have been used to determine the branching ratio of the two decays:

$$BR_{0^+ \rightarrow 0^+} = 87.3(35) \% \quad (1)$$

$$BR_{0^+ \rightarrow 2^+} = 12.7(35) \% \quad (2)$$

The large uncertainty on the detection efficiency of especially the 143.5 keV gamma leads to a large uncertainty in the final result of the branching ratio. The result is consistent with the values of 82.3(15)% and 17.7(15)% determined earlier [19].

The time signal also enabled a determination of the lifetime of the 0_2^+ state using the time difference spectrum for the 511 keV gamma line, Fig. 5D. The spectrum is fitted to an exponential decay and gives a lifetime of:

$$\tau = 357(22) \text{ ns.}$$

The value is in good agreement with the value ($\tau = 331(12)$ ns) determined by Shimoura et al. [19].

The last peak (green) in Fig. 4C is made by gating on the two time delayed gamma peaks. Again the mean value of the excitation energy peak at 2200 keV validates the two gamma gates as stemming from the decay of the 0_2^+ state. The spectra is scaled with a factor $1/0.63$ in addition to the $1/\epsilon$ from Table I. This extra factor of $1/0.63$ stems from the additional timegate ($dt > 100$ ns). For an exponential decay with a lifetime of 357 ns, only 63% of the decays will be within the time window of [100 ns, 750 ns].

To test for the presence of other components in the total excitation energy spectrum Fig. 4D shows the spectra in Fig. 4B with the gamma gated spectra subtracted. Most of the events above the ground state have disappeared, indicating that with the applied scaling, the gamma gated spectra can be used for cross section calculation without any major uncertainty in the overall amplitude. A small part of the total spectrum is still unaccounted for, which most likely stems from an unaccounted background, either from a small contamination of ^{22}Ne in the beam or extra contaminations in the target. The possibility of some small extra components of the three excited states can not be ruled out though. Especially the 0_2^+ state might not be fully described by the gamma gate, due to the requirement of a stopped ^{12}Be nucleus for the gamma detection. Furthermore, the detection efficiency (ϵ) in Table I is determined for decays occurring at the target position not in the detectors at

the end of the setup, which could lead to a slight change in the scaling. Hence, the additional background leads to an extra uncertainty in the absolute amplitude of the cross sections for the two 0^+ states. This is reflected in the uncertainties of the final spectroscopic factors, Table III.

B. Search for further bound states

The extra data not accounted for by the gamma gated excitation energy spectra could also stem from a yet unseen bound state in ^{12}Be . A bound 0_1^- state is predicted in a three-body model [28]. The excitation energy of the state is estimated to be between 2.1 MeV and 3.1 MeV in the model. Any 0_1^- state above the 1_1^- state can be ruled out by the data presented here. All events with excitation energy above 2.7 MeV are described by the gamma gated spectra, Fig. 4D. Furthermore, there is no gamma line between 100 keV and 400 keV in Fig. 5A. The only peak present is the unknown background peak at 166 keV. This narrows the energy search to the interval between 2.1 MeV and 2.7 MeV. This interval can be further narrowed down. A 0_1^- state between the 2_1^+ and the 1_1^- state would mainly decay to the 2_1^+ state with an M2 transition. The state will then be long lived with a lifetime comparable to the 0_2^+ state. Hence a peak between 200 keV and 500 keV should emerge in the black spectrum shown in Fig. 5C, like the 511 keV and the 143.5 keV lines. No extra peak is seen in the spectra. From this we can limit the possible energy range for a bound 0_1^- state to:

$$E^* \in [2.1 \text{ MeV}, 2.2 \text{ MeV}]. \quad (3)$$

From Fig. 4D we can determine the population strength for an additional state at 2.15 MeV to be more than a factor of 10 less than the 1_1^- state. This would not be the case for a 0^- state, that only differs from the 1_1^- state in spin coupling. Therefore, it is very unlikely, that a bound 0^- state exists in ^{12}Be .

C. Particles stopped in the forward ΔE -detector

Studying the particles stopped in the ΔE -detectors is the next step. We first consider the forward laboratory angles. All protons producing ^{12}Be in the ground state go through the ΔE -detector in forward angles, see Fig. 2B. This leaves only the protons to excited states in ^{12}Be to be identified. The population of the excited states can be determined using the same gates as in the previous section. Fig. 6A shows the Doppler-corrected gammas in coincidence with particles stopped in the ΔE and Fig. 6B shows the laboratory gamma energy before (red) and after (black) the reaction. The plots are similar to Fig. 5A+C. More peaks appears in the Doppler-corrected spectrum. These gammas stem mainly from inelastic

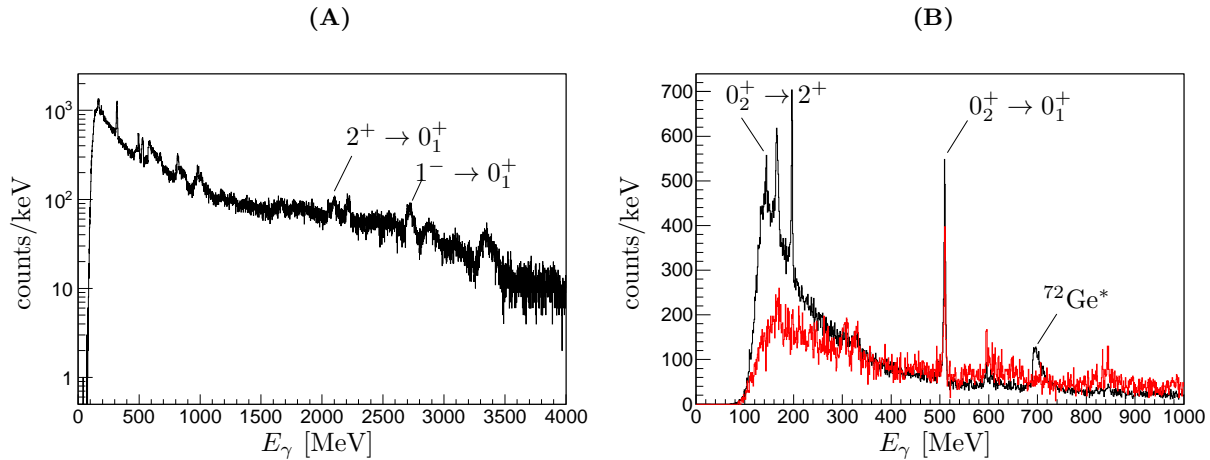


FIG. 6. E_γ -spectra for gammas in coincidence with unidentified charged particles stopped in the ΔE -detectors. A: Doppler-corrected energy spectrum. B: Laboratory gamma energy spectra for gammas emitted before (red) and after (black) the reaction. The time gates are similar to the ones in Fig. 5C.

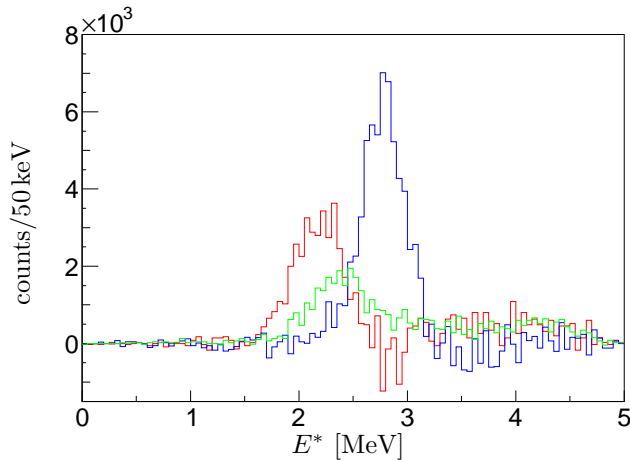


FIG. 7. The excitation energy of ^{12}Be determined from the momentum of particles stopped in the ΔE -detectors in the forward angles and gated on the gamma lines shown in Fig. 6. Red: 2_1^+ , green: 0_2^+ and blue 1_1^- .

scattered ^{11}Be ($E_\gamma = 320\text{ keV}$), excited states in ^{10}Be populated in (d,t)-reactions ($E_\gamma = 2590\text{ keV}$, 2812 keV and 3367 keV) and reactions on C and H. The two peaks at 2096 keV and 2723 keV are still present and easily separable from other gamma lines.

Comparing the laboratory gamma energy spectra before and after the reaction time shows the same appearance of the three peaks mentioned in the previous section. Two things should be noted. A fourth peak at 197 keV appears after the reaction point. The peak stems from decays in ^{19}F populated in reactions of ^{11}Be on ^{12}C in the target. Secondly, a significant peak at 511 keV is seen before the reaction time. This indicates a non-negligible background from positrons within the ISOLDE experimental hall. This leads to a significant background when

using the gate, which is taken into account when producing the gamma gated excitation energy spectrum, Fig. 7. All three gamma gated spectra in Fig. 7 are peaked at the correct excitation energies and the background which remains is negligible.

D. Particles stopped in the backward ΔE -detector

The last part of the analysis concerns the backward laboratory angles. Protons producing ^{12}Be in the ground state are the only ones detected in the backward angles, due to the high lower energy detection threshold, Fig. 2B. An excitation energy spectrum is made from all particles stopped in the ΔE detector in backward angles. All particles are assumed to be protons, Fig. 8A. Background from C and H in the target are subtracted using the runs on pure carbon and regular polyethylene targets, Fig. 8B. The ground state is clearly seen, but a significant background is still present. The background leads to a larger uncertainty in the determined differential cross sections for the small center of mass angles.

IV. RESULTS

The experimental differential cross sections for the (d,p)-population of the four bound states are determined by comparing the excitation energy spectrum, determined in section III, with a geant4 [45] simulation. This simulation was done using the g4miniball package [42]. The gamma gated excitation energy spectra from Fig. 4C and 7 are used for the excited states (2_1^+ , 0_2^+ and 1_1^-). The total excitation energy spectra from Fig. 4 and 8 are used for the ground states. The experimental differential cross sections are shown in Fig. 9 (red dots).

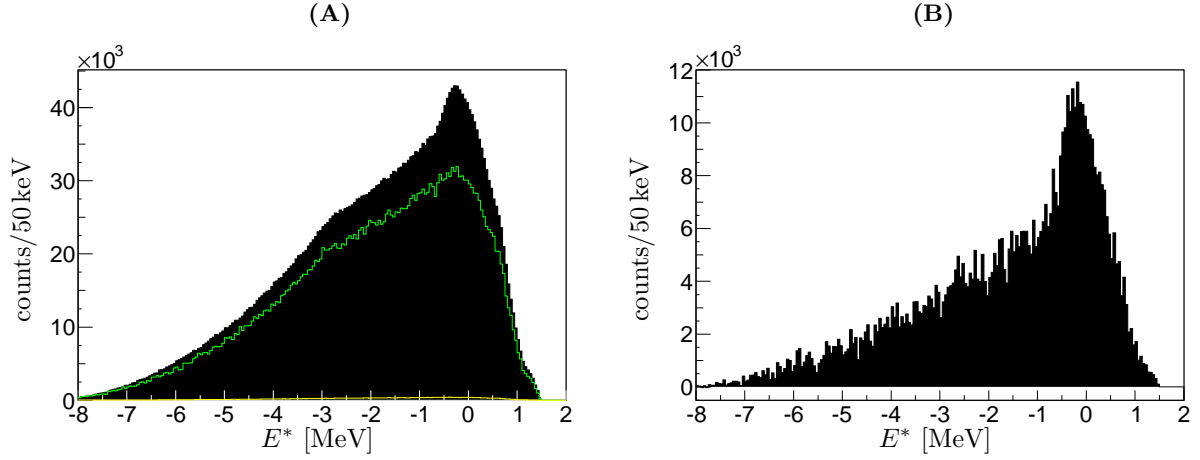


FIG. 8. Excitation energy spectra of ^{12}Be calculated for particles in backward laboratory angles. A: The total excitation energy spectrum (black) along with the background spectra from runs on the carbon target (green) and the CH₂ target (yellow). B: The excitation energy spectrum with the two background spectra subtracted.

Channel	set	V_0	r_0	a_0	δ_1	δ_2	W_v	W_d	r_I	a_I	V_{so}	r_{so}	a_{so}
$^{12}\text{Be}+p$	I+II+III	57.8	1.25	0.25	0	0	0	8.08	1.4	0.22	6.5	1.25	0.25
	IV	58.59	1.12	0.67	0	0	0.85	5.26	1.3	0.51	5.53	0.90	0.59
$^{11}\text{Be}+d$	I	124.7	0.9	0.9	0	0	0	4.38	2.452	0.264	6.0	0.9	0.9
	II	120.18	0.9	0.9	0.84	1.27	0	19.535	2.452	0.264	6.0	0.9	0.9
	III	118.0	0.87	0.91	0	0	0	5.80	1.57	0.78	5.80	0.87	0.91
	IV	80.53	1.17	0.8	0	0	5.19	4.71	1.56	0.8	3.54	1.23	0.81
$^1\text{H}+n$		72.15	1.484										
$^{11}\text{Be}+n$		54.14	1.35	0.9							8.50	1.35	0.9

TABLE II. Parameters for the six optical potentials used in the four (I-IV) DWBA calculations along with the two binding potentials for ^2H and ^{12}Be . All potentials have a Wood-Saxon shape except the $^1\text{H}+n$ potential, which is a Gaussian shape.

Theoretical calculations of the differential cross sections are needed in order to extract conclusions from the experimental results. This step is complex in our case, partly because the “forward peak” is only covered for the ground state transition, partly because both initial nuclei — the deuteron and ^{11}Be — are loosely bound systems. The theory for (d,p) reactions is still being refined for challenging cases like this and is often making use of continuum discretized coupled channel (CDCC) calculations, see [46–48] and references therein. The concept of a spectroscopic factor, often used earlier as the key quantity to be extracted from experiment, has also been questioned during the last decade, see Mukhamedzhanov [48] and Jennings [49] for recent overviews, asymptotic normalization coefficients (ANC) [48, 50–52] have been used instead. A proper theoretical analysis of our data is beyond the scope of the present paper so we shall here just briefly indicate what can be learned from a standard approach to allow comparison with earlier experimental work [25].

The differential cross sections are compared to distorted wave Born approximation (DWBA) calculations performed with FRESKO [53, 54]. Four DWBA calculations are performed using the parameters from Table II.

The interaction potentials are of the form:

$$V(r) = -V_0 f(x_0) - i \left(W_v f(x_I) - W_d \frac{df((x_I))}{dx_I} \right) + V_{so} \frac{\hbar^2}{m_\pi c r} \frac{1}{dx_{so}} \frac{df((x_{so}))}{dx_{so}} (\vec{L} \cdot \vec{s})$$

where $f(x)$ is the Wood-Saxon:

$$f(x_i) = \frac{1}{1 + \exp(x_i)} \\ x_i = \frac{r - r_i A^{1/3}}{a_i}.$$

The $^{12}\text{Be}+p$ potentials are taken from reference [55] (set I+II+III) and [56] (set IV). The first $^{11}\text{Be}+d$ potential is calculated from generalized parameters given by Satchler et al. [57] (set I). The depths of this potential is modified for the second set (set II) and a deformation taken from Hussein et al. [58] is added. The second potential fits better the elastic scattered deuterons (not investigated here). The last two ^{11}Be potentials are taken from Fitz et al. [59] and Han et al. [60]. These two potentials were used in combination with the two $^{12}\text{Be}+p$ potentials to investigate the differential cross sections from

State	set I	set II	set III	set IV
0_1^+	$0.15^{+0.03}_{-0.05}$	$0.25^{+0.05}_{-0.08}$	$0.15^{+0.03}_{-0.05}$	$[0.30^{+0.20}_{-0.22}]$
2_1^+	0.15(5)	0.30(10)	0.075(25)	0.40(10)
0_2^+	$[0.40^{+0.14}_{-0.10}]$	$[0.32^{+0.12}_{-0.09}]$	$0.40^{+0.13}_{-0.09}$	$[0.95^{+0.43}_{-0.36}]$
1_1^-	$[0.55(20)]$	$[0.50(20)]$	$[0.27(15)]$	$[0.85(35)]$

TABLE III. Spectroscopic factors for the four bound states in ^{12}Be . The spectroscopic factors are given for each set of parameters shown in Table II. Square brackets indicate cases where the angular shapes do not match.

the $^{11}\text{Be}(d,p)^{12}\text{Be}$ experiment performed at TRIUMF by Kanungo et al. [25].

The two binding potentials are taken from Austern et al. [61] for $^1\text{H}+n$ and Nunes et al. [62] for $^{11}\text{Be}+n$. The $^{11}\text{Be}+n$ potential has a Wood-Saxon shape and the $^1\text{H}+n$ has a Gaussian form:

$$V(r) = V_o \exp \left[(r/r_o)^2 \right].$$

The parameters can be seen in Table II.

The theoretical differential cross sections for each of the four sets of parameters are plotted in Fig. 9. The deduced spectroscopic factors from the four calculations are given in Table III.

The cross sections from set IV can only reproduce the shape of the 2_1^+ cross section and the validity of these parameters is very questionable. The first three sets reproduces the ground state well and to a large extent the 2_1^+ state. Only set III can reproduce the shape for the 0_2^+ state and none of the potentials can reproduce the shape for the 1_1^- . The low binding energy and the possible two-halo structure of the 1_1^- state is expected to play an important role in the reaction mechanism to the 1_1^- . The overall agreement is not satisfactory, but as mentioned above this is not too surprising and a better description of the reaction mechanisms is needed where effects due to the halo structure of the two initial nuclei, e.g. break-up of the halo [47, 63], are included.

The deduced spectroscopic factors are highly model dependent as seen in Table III. The values from the three first sets are generally consistent and are used to obtain average spectroscopic factors. The last set is omitted due to the poor agreement with the experimental differential cross sections. The average spectroscopic factors are given in Table IV along with spectroscopic factors determined by Kanungo et al. [25] and from two theoretical models: a shell model calculation made by H. Fortune et al. [64] and a three-body model calculation made by E. Garrido et al. [65]. Effects of core excitation are not yet included in the three-body model [65]. The experimentally determined spectroscopic factors of the 2_1^+ and the 1_1^- states are in good agreement. The factor of two between the ground state spectroscopic factors may be due to the different potentials used. For the excited 0_2^+ state the previous determination carried a large uncertainty since the 2_1^+ and the 0_2^+ states could not be separated in [25]. The states are identified and separately analyzed in

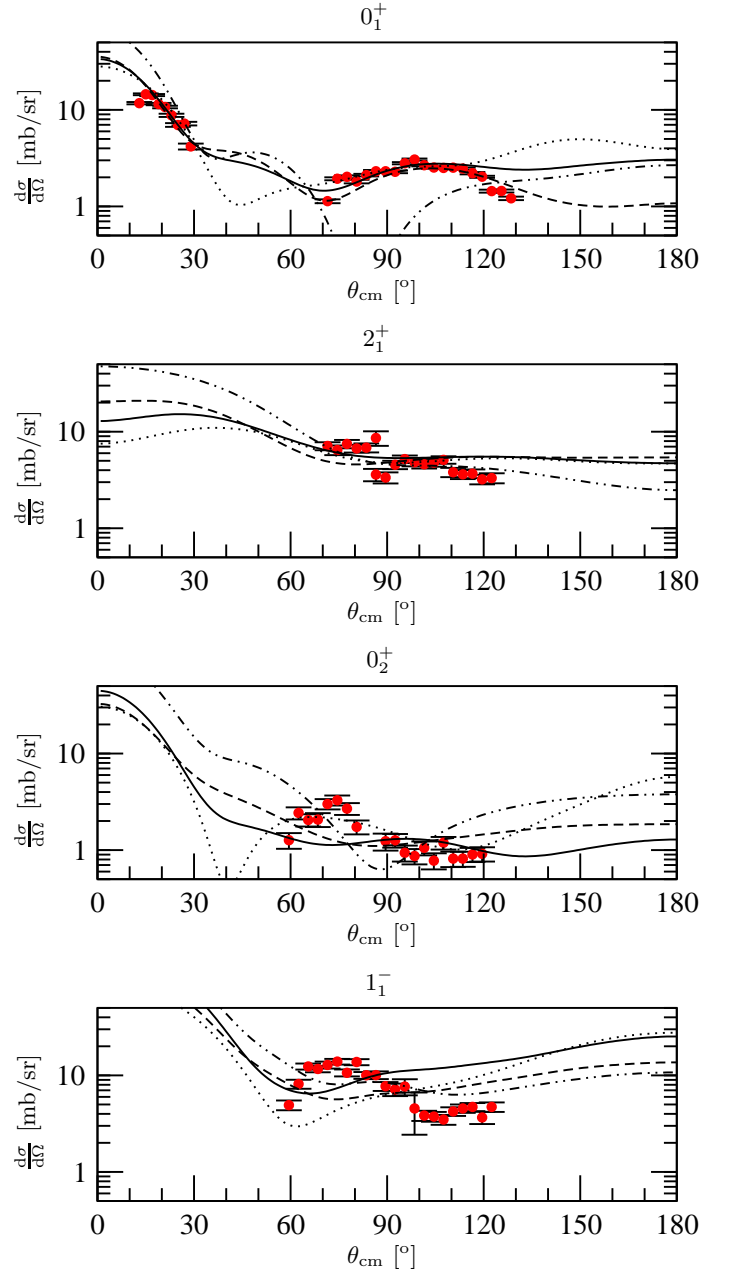


FIG. 9. The experimentally determined differential cross sections for the four bound states in ^{12}Be (red dots). The DWBA calculations are plotted on top of the experimental data; set I: full line (—), II: dashed (---), III: dotted (...) and IV: dash-dotted (-.-).

this experiment and this should provide a more reliable value for the 0_2^+ state.

The experimental spectroscopic factor is, in contrast to the theoretical ones, larger in the excited 0_2^+ state than the ground state; this and the overall large disagreement between the experimental determined spectroscopic factors and the theoretical ones is still to be understood.

State	This work	Ref. [25]	Ref. [64]	Ref. [65]
0_1^+	$0.17^{+0.04}_{-0.07}$	$0.28^{+0.03}_{-0.07}$	0.78	0.60
2_1^+	0.15(5)	$0.1^{+0.09}_{-0.07}$	0.52	(0.35)
0_2^+	$0.40^{+0.13}_{-0.10}$	$0.73^{+0.27}_{-0.40}$	0.37	0.07
1_1^-	0.5(2)	≈ 0.35	—	0.50
0_1^-	—	—	—	0.53

TABLE IV. Four spectroscopic factors for each of the four bound states in ^{12}Be . The four sets stem from; this experiment, a $^{11}\text{Be}(\text{d},\text{p})$ experiment performed at TRIUMF [25], a shell model calculation [64] and a three-body calculation [65].

V. SUMMARY AND CONCLUSION

The combined power of the T-REX and MINIBALL arrays allows to identify individual final states in the $^{11}\text{Be}(\text{d},\text{p})^{12}\text{Be}$ reaction. All previously known excited bound states have been seen through observation of gamma rays from their decay. For the decay of the 0_2^+ state the lifetime has been measured to $\tau = 357(22)\text{ ns}$ and the branching ratios of the decays to the ground state and the 2_1^+ state have been determined to $BR_{0^+ \rightarrow 0^+} = 87.3(35)\%$ and $BR_{0^+ \rightarrow 2^+} = 12.7(35)\%$ respectively. These values are in good agreement with previously determined values. No indications for new bound states were seen, there are in particular no indications for the presence of a bound 0_1^- state. The excitation energy of such a bound state has been limited to be between the 2_1^+ and the 0_2^+ state in an interval of only 100 keV. The amount of unaccounted data within this interval will lead to a population strength much below that expected for a bound 0_1^- state. Hence a fifth bound state in ^{12}Be can be ruled out.

Differential cross sections have been extracted over a large angular range (60° to 120° in the center-of-mass system) and compared to four different sets of DWBA

calculations in order to determine spectroscopic factors. None of the DWBA calculations could reproduce all of the experimental differential cross sections. The difference between the experimental and theoretical differential cross sections is large, especially for the high lying levels. This may be due to the loosely bound neutrons in the initial states and the suggested halo structure of some of the final states, factors which are known to affect the reaction mechanism. More refined calculations must be made for the theoretical differential cross sections, e.g. CRC found to be essential to describe the $^8\text{Li}+^2\text{H}$ reaction at a similar energy [52]. The current disagreement between theoretical and experimental spectroscopic factors may be due to the simplicity of the DWBA calculations, but it is disturbing that the relative strength of transitions to the two 0^+ states has opposite trends for theory and experiment. It will clearly be important to go beyond the simple theoretical treatment presented here.

Acknowledgments: This work was supported by the European Union Seventh Framework through ENSAR (contract no. 262010), by the BMBF under the contracts 06MT7178, 06MT9156, 05P09PKCI5, 05P12PKFNE, 06DA9036I and 05P12RDCIA, by the Spanish MICINN under the contracts FPA2010-17142 and FPA2012-34332, by the FWO-Vlaanderen (Belgium), by GOA/10/010 (BOF KU Leuven), by the Interuniversity Attraction Poles Programme initiated by the Belgian Science Policy Office (BriX network P7/12), by the United Kingdom Science and Technology Facilities Council, by a Marie Curie Intra-European Fellowship of the European Community's 7th Framework Programme under contract number PIEF-GA-2008-219175, and by Maier-Leibnitz-Laboratorium, Garching. The authors would like to thank Aksel S. Jensen and Eduardo Garrido for valuable inputs and discussions regarding the nuclear structures. We would also like to thank Antonio M. Moro for his input regarding the theoretical calculations of the differential cross sections.

-
- [1] B. Jonson, Phys. Reports 389, 1 (2004)
 - [2] A.S. Jensen, K. Riisager, D.V. Fedorov and E. Garrido, Rev. Mod. Phys. 76, 215 (2004)
 - [3] I. Tanihata, H. Savajols and R. Kanungo, Prog. Part. Nucl. Phys. 68, 215 (2013)
 - [4] K. Riisager, Phys. Scr. T152, 014001 (2013)
 - [5] W. von Oertzen, M. Freer and Y. Kanada-Eny'o, Phys. Reports 432, 43 (2006)
 - [6] T. Baumann, A. Spyrou and M. Thoennessen, Rep. Prog. Phys. 75, 036301 (2012)
 - [7] H. Simon, Phys. Scr. T152, 014024 (2013)
 - [8] R. Kanungo, Phys. Scr. T152, 014002 (2013)
 - [9] K. Blaum, J. Dilling and W. Nörtershäuser, Phys. Scr. T152, 014017 (2013)
 - [10] T. Aumann and T. Nakamura, Phys. Scr. T152, 014012 (2013)
 - [11] N. Keeley, R. Raabe, N. Alamanos and J.L. Sida, Prog. Part. Nucl. Phys. 59, 579 (2007)
 - [12] K. Wimmer *et al.*, Phys. Rev. Lett. 105, 252501 (2010)
 - [13] A. Bonaccorso, Phys. Scr. T152, 014019 (2013)
 - [14] K.L. Jones, Phys. Scr. T152, 014020 (2013)
 - [15] K.T. Schmitt *et al.*, Phys. Rev. Lett. 108, 192701 (2012)
 - [16] F.C. Barker, J. Phys. G2, L45 (1976)
 - [17] H. Iwasaki *et al.*, Phys. Lett. B491, 8 (2000)
 - [18] S. Shimoura *et al.*, Phys. Lett. B560, 31 (2003)
 - [19] S. Shimoura *et al.*, Phys. Lett. B654, 87 (2007)
 - [20] N. Imai *et al.*, Phys. Lett. B673, 179 (2009)
 - [21] A. Krieger *et al.*, Phys. Rev. Lett. 108, 142501 (2012)
 - [22] A. Navin *et al.*, Phys. Rev. Lett. 85, 266 (2000)
 - [23] S.D. Pain *et al.*, Phys. Rev. Lett. 96, 032502 (2006)
 - [24] W.A. Peters *et al.*, Phys. Rev. C83, 057304 (2011)
 - [25] R. Kanungo *et al.*, Phys. Lett. B682, 391 (2010)
 - [26] R. Meharchand *et al.*, Phys. Rev. Lett. 108, 122501 (2012)
 - [27] C. Romero-Redondo, E. Garrido, D.V. Fedorov and A.S. Jensen, Phys. Rev. C77, 054313 (2008)

- [28] C. Romero-Redondo, E. Garrido, D.V. Fedorov and A.S. Jensen, Phys. Lett. B660, 32 (2008)
- [29] H.T. Fortune and R. Sherr, Phys. Rev. C85, 051303 (2012)
- [30] Y. Kanada-En'yo and H. Horiuchi, Phys. Rev. C68, 014319 (2003)
- [31] I. Hamamoto and S. Shimoura, J. Phys. G34, 2715 (2007)
- [32] M. Dufour, P. Descouvemont and F. Nowacki, Nucl. Phys. A836, 242 (2010)
- [33] H.T. Fortune, G.-B. Liu and D.E. Alburger, Phys. Rev. C50, 1355 (1994)
- [34] H.B. Jeppesen *et al.*, Nucl. Phys. A748, 374 (2005)
- [35] E. Garrido, A.S. Jensen, D.V. Fedorov and J.G. Johansen, Phys. Rev. C86, 024310 (2012)
- [36] V.N. Fedoseyev, G. Huberg, U. Köster, J. Lettry, V.I. Mishin, H. Ravn and V. Sebastian, Hyperfine Int. 127, 409 (2000)
- [37] O. Kester *et al.*, Nucl. Instr. Meth. Phys. Res., sect B204, 20 (2003)
- [38] J.G. Johansen, M.A. Fraser, V. Bildstein, T. Kröll, R. Raabe, K. Riisager, D. Voulot and K. Wimmer, Nucl. Instr. Meth. A714, 176 (2013)
- [39] J.G. Johansen, Ph.D. thesis, Aarhus University (2012), CERN-THESIS-2012-282
- [40] J. Eberth *et al.*, Prog. Part. Nucl. Phys. 46, 389 (2001)
- [41] N. Warr *et al.*, Eur. Phys. J. A49: 40 (2013)
- [42] V. Bildstein *et al.*, Eur. Phys. J. A48: 85 (2012)
- [43] C. Chasman, K.W. Jones and R.A. Ristinen, Nucl. Instr. Meth. 37, 1 (1965)
- [44] D.G. Jenkins *et al.*, Nucl. Instr. Meth. A602, 457 (2009)
- [45] S. Agostinelli *et al.*, Nucl. Instr. Meth. A506, 250 (2003)
- [46] N. Keeley, N. Alamanos and V. Lapoux, Phys. Rev. C69, 064604 (2004)
- [47] A.M. Moro, F.M. Nunes and R.C. Johnson, Phys. Rev. C80, 064606 (2009)
- [48] A.M. Mukhamedzhanov, Phys. Rev. C84, 044616 (2011)
- [49] B.K. Jennings, arXiv:1102.3721
- [50] A.M. Mukhamedzhanov and R.E. Tribble, Phys. Rev. C59, 3418 (1999)
- [51] N.K. Timofeyuk, R.C. Johnson and A.M. Mukhamedzhanov, Phys. Rev. Lett. 91, 232501 (2003)
- [52] E. Tengborn *et al.*, Phys. Rev. C84, 064616 (2011)
- [53] I.J. Thompson, Computer Physics Reports 7, 167 (1988)
- [54] I.J. Thompson and F.M. Nunes, Nuclear Reactions for Astrophysics, Cambridge University Press (2009)
- [55] J.R. Comfort and B.C Karp, Phys Rev C21, 2162 (1980)
- [56] A.J. Koning, J.P. Delaroche, Nucl. Phys. A713 (2003) 231
- [57] G.R. Satchler, Nucl. Phys. 85, 273 (1966)
- [58] M.S. Hussein and R. Lichtenthäler, Phys. Rev. C77, 054609 (2008)
- [59] W. Fitz, R. Jahr and R. Santo, Nucl. Phys. A101 (1967) 449
- [60] Y. Han, Y. Shi and Q. Shen, Phys. Rev. C 74 (2006) 044615
- [61] N. Austern *et al.*, Phys. Rep. 154, 125 (1987)
- [62] F. Nunes *et al.*, Nucl. Phys. A609, 43 (1996)
- [63] A.M. Moro and R. Crespo, Phys. Rev. C85, 054613 (2012)
- [64] H.T. Fortune and R. Sherr, Phys. Rev. C83, 044313 (2011)
- [65] E. Garrido *et al.*, to be published